



Efficient implementation on accuracy improvement of the two-dimensional node-to-segment contact approach for explicit dynamic analysis

Seung-Hoon Kang¹ · Seok-Min Lee² · SangJoon Shin^{1,3}

Received: 2 August 2023 / Accepted: 23 November 2023
© The Author(s) 2023

Abstract

The penalty-method-based node-to-segment (NTS) approach is widely employed in the explicit dynamic analysis owing to its computational efficiency and implementation simplicity. However, the classical approach does not pass the contact patch test and results in severe inaccuracies. This study attempts the accuracy enhancement of an explicit dynamic contact analysis with minimum efficiency loss using the NTS algorithm with the modified area regularization technique (NTS-mAR). The computational procedure is compared to an allied modified penalty-method-based NTS approach, i.e., the virtual node-to-segment algorithm passing the patch test (VTS-PPT). Then, an extension to an explicit dynamic analysis framework is attempted, wherein the speed of the contact force calculation significantly influences the overall computational efficiency. The cost of the remaining computation was minimized by employing a lumped mass matrix and a one-point integration rule for the internal force. Elastoplasticity was considered to extend its application. The accuracy improvement compared to the classical one-pass NTS approach was similar for the modified approaches. The VTS-PPT approach requires more than twice the cost of contact force estimation compared with the classical one-pass NTS approach. In contrast, NTS-mAR approach induces a cost increase from 6 to 36% that of classical one-pass NTS approaches. For the given examples, the NTS-mAR approach is beneficial when an improvement in accuracy is desired with minimum efficiency loss.

Keywords Contact algorithm · Penalty method · Modified node-to-segment approach · Explicit dynamic analysis · Computational speed

1 Introduction

Contact analysis using the finite element (FE) method typically involves a non-conformally discretized interface. For such complicated situations, the node-to-segment (NTS) approach [1–5] is used. This overcomes the node-matching

limitations of the conventional node-to-node approach and allows for a large deformation and sliding contact scenario.

This study focuses on the NTS approach combined with the penalty method [6, 7]. Unlike the Lagrange multiplier method under exact contact enforcement, the penalty method allows penetration between the slave and master bodies. Such a slight violation eliminates the need for additional variables, such as the Lagrange multiplier, and simplifies the NTS approach. LS-DYNA [8] and Radioss [9] are representative commercial FE software that employ a penalty method for the contact-impact simulation.

However, the classical one-pass NTS approach fails the contact patch test [10]. Several remedies have been proposed for penalty formulation, independent of those for the Lagrange multiplier method [11–17]. This is because the inaccuracy of the penalty method is primarily due to the characteristics of the penalty parameters. The underlying idea is to revise the constant penalty parameter so that it varies along the contact elements while considering the geometric

✉ SangJoon Shin
ssjoon@snu.ac.kr

Seung-Hoon Kang
shkang94@snu.ac.kr

Seok-Min Lee
stone_m_lee@hyundai.com

¹ Department of Aerospace Engineering, Seoul National University, Seoul 08826, Republic of Korea

² R&D Division, Hyundai Motor Company, Hwaseong-si, Gyeonggi-do 18280, Republic of Korea

³ Institute of Advanced Aerospace Technology, Seoul National University, Seoul 08826, Republic of Korea

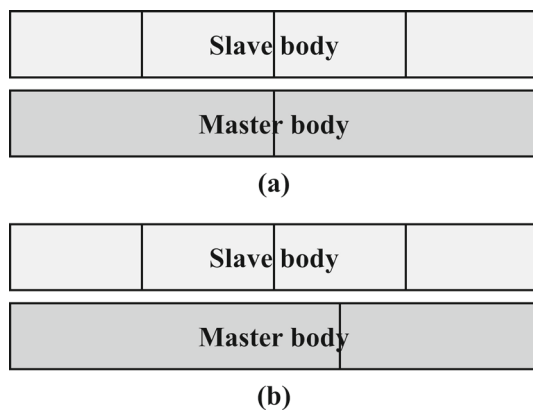


Fig. 1 Nonconformally discretized contact interface: **a** normal and **b** pathologic cases

or material properties. The area regularization (AR) technique [18, 19] attempts to vary the penalty parameters in proportion to the competence area of the slave node. Lee [20] and Lee et al. [21] investigated the NTS approach using the AR technique (NTS-AR) in a three-dimensional dynamic condition. An examination of the frictional contact analysis is presented in Ref. [22]. The NTS-AR approach improved the accuracy of the classical one-pass NTS approach. It passed the *normal* [19] contact patch test (Fig. 1a), in which all slave nodes of each segment are projected upon a single master segment. Moreover, LS-DYNA [23] functionally scales the penalty parameter in terms of area, mass, or shell thickness.

Nevertheless, the aforementioned methods did not pass the contact patch test for the so-called *pathologic* [19] situation (Fig. 1b), in which the slave segment spans multiple master segments. This limitation was overcome by improving the NTS-AR approach to consider both slave and master geometries. Zavarise and De Lorenzis [19] proposed a virtual node-to-segment approach that passed the patch test (VTS-PPT). In this approach, the competence area of the virtual node inside the slave segment is projected onto the master segment and is utilized as a penalty weighting factor. The contact force is distributed to the projected master segments in accordance with the projected area.

The segment-to-segment (STS) [12, 24–26] and mortar [27–36] approaches have been actively investigated over the past few decades. These are well-established and have been implemented in several FE software programs [8, 37], exhibiting a high level of accuracy and stability. However, they require significant computational costs, which is contrary to the NTS approach, despite recent efforts for efficient contact simulation [38–40]. In this context, the classical one-pass NTS and allied modified approaches are expected to play a major role when computational efficiency is desired with moderate accuracy.

Recently, as another variant of the penalty-method-based NTS approach, Kang et al. [41] proposed a NTS-AR

approach combined with a partial dual-pass scheme. This is equivalent to the original NTS-AR approach in a normal situation. For the pathologic situation, the master nodes between the slave projections additionally act as contact elements, which take part of the slave penalty weighting factor. For convenience, this is referred to as the NTS approach with modified AR technique (NTS-mAR). NTS-mAR passed the contact patch test with an improved accuracy equivalent to that of the VTS-PPT approach. Furthermore, the absence of a supplementary virtual node reinforced the simplicity of implementation. However, the validation of NTS-mAR was conducted within the implicit analysis in terms of accuracy.

For the modified NTS approaches of mid-fidelity to be competitive in practice, efficient computation should be achieved. Based on preliminary studies [41, 42], this study attempted to extend NTS-mAR approach to an dynamic analysis including the elastoplasticity and investigated its overall competitiveness. First, the overall procedure is described and compared with allied NTS approaches. Subsequently, the computational efficiency is examined in the explicit dynamic analysis framework with a lumped mass matrix. Within such a framework, the cost of contact force computation becomes more crucial than that in implicit analysis because it excludes the linear algebraic solver for global matrix computation. To compute the internal force vector, dynamic analysis is combined with the quadrilateral element of the one-point integration rule. An elastoplastic model was considered to include material nonlinearity. VTS-PPT, the evaluation of which was also confined within the implicit static context [19], is further extended to the same dynamic analysis framework for the comparison.

2 Classical and modified NTS approaches

This section introduces the preliminaries of the classical one-pass NTS and its modified approaches. In this study, the formulation and analysis of contact approaches are presented in a two-dimensional frictionless condition. The FE of the linear interpolation function was employed because the modified approaches, VTS-PPT and NTS-mAR, have been formulated for linear interpolation [19, 41]. This is also because the classical one-pass NTS approach generally deals with the linearly interpolated FE [11].

2.1 Classical one-pass NTS approach

Figure 2 illustrates the contact element of the classical penalty-method-based NTS approach. The slave node S on the slave contact surface Γ_c^{sl} penetrates the master segment M_1M_2 on the master contact surface Γ_c^{ms} . Subsequently, a negative gap or penetration g_N occurs along the unit normal vector on the master segment \mathbf{n} . Here, \mathbf{n} originates from the

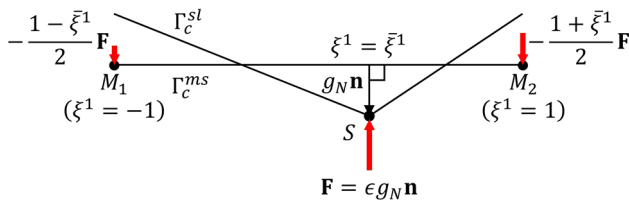


Fig. 2 Contact element of the classical one-pass penalty-method-based NTS approach

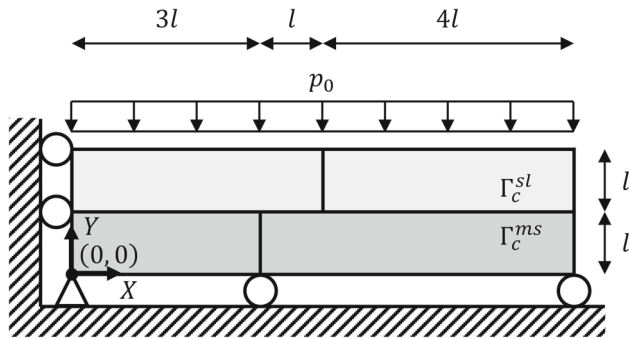


Fig. 3 Schematic of the patch test

closest point projection $\xi^1 = \bar{\xi}^1$ from S to $\overline{M_1M_2}$, whose position is expressed by the contravariant convective coordinate ξ^1 . The contact force at the slave node is determined as $\mathbf{F} = \epsilon g_N \mathbf{n}$, where ϵ denotes the penalty coefficient. For master nodes M_1 and M_2 , the contact force is applied in the opposite direction proportional to each linear interpolation function based on the projection $\xi^1 = \bar{\xi}^1$. A detailed explanation of the NTS approach is provided in Refs. [5–7].

The classical one-pass NTS approach with a constant penalty coefficient along the slave nodes does not pass the contact patch test. This paper presents a simple case to supplement previous studies [19, 41] that extensively discussed this drawback through numerous patch test cases. Figure 3 shows the patch tests for two identical rectangular blocks. A uniformly distributed pressure of $p_0 = 1 \text{ N/m}$ was applied to the upper block, and the upper block sequentially pressed the lower block. Here, the length l , elastic modulus E , and Poisson’s ratio ν were set as 1 m, 1 MPa, and 0, respectively. The upper and lower surfaces were designated as the slave and master surfaces, respectively. The analytical solution along the interface is a uniform contact pressure, that is, a contact force that achieves the local equivalence of the force and moment. The corresponding penetration is also uniform. The patch test validation checked if the assumption of uniform penetration resulted in a uniform contact pressure.

Figure 4 depicts the penalty parameter distribution and the corresponding contact force applied to each segment for uniform penetration g_N . When a contact force is applied to a node between two segments, it is distributed proportionally to the segment area. As shown, the NTS approach does

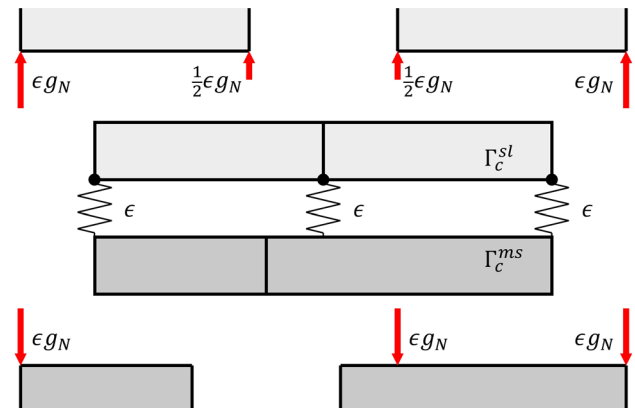


Fig. 4 Patch test of the classical one-pass NTS approach for uniform penetration: contact force distribution

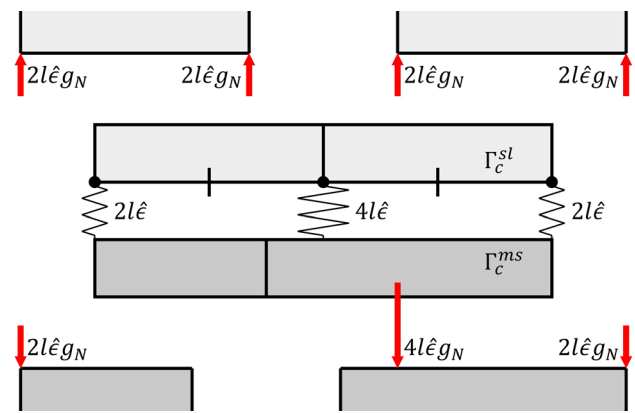


Fig. 5 Patch test of one-pass NTS-AR approach for the uniform penetration: contact force distribution

not achieve local moment equivalence of the slave segments. This is because the constant penalty parameter ϵ ignores the discretization characteristics of the slave surface and those of the master segments that include both force and moment nonequivalence.

The NTS-AR approach [18–23] provides a simple solution for reflecting slave surface discretization. It employs a distributed penalty parameter $\hat{\epsilon}$ and allocates the parameter ϵ according to the competence area of each slave node. Here, the competence area of a node is the sum of half the areas of the neighboring segments. As shown in Fig. 5, the local nonequivalence of the slave segments is resolved. However, that of the master segments persists because the NTS-AR approach does not consider the discretization of the master surface, as the classical one-pass NTS approach.

Figure 6 shows the results of the numerical simulation, wherein the contact pressure p was nonuniform. Here, the previous assumption of uniform penetration is removed. Therefore, for a contact approach that does not pass the patch test, the penetration varies with the slave nodes to achieve global equivalence, as shown in Fig. 7. Because the mag-

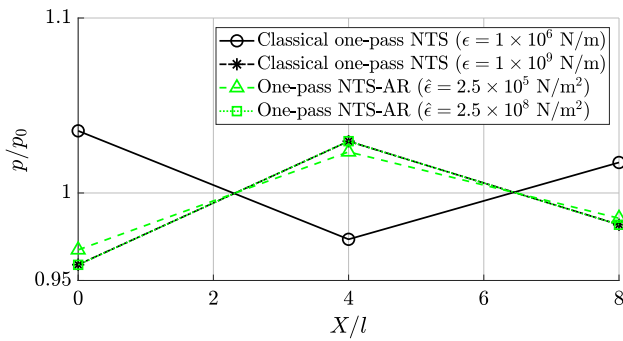


Fig. 6 Patch test of the classical one-pass NTS and NTS-AR approaches via numerical simulation: contact pressure along the slave surface

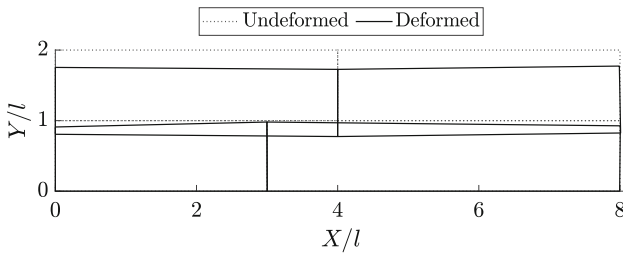


Fig. 7 Patch test of the classical one-pass NTS approach via numerical simulation: deformed configuration for $\epsilon = 1 \times 10^6$ N/m. Scale factor for the deformation is 5×10^4

nitude of nonuniform penetration depends on the penalty parameter, the contact pressure distribution varies accordingly.

2.2 Modified NTS approaches

The VTS-PPT [19] and NTS-mAR [41] approaches resolve the aforementioned local nonequivalence by considering the geometries of both the slave and master surfaces. However, the relevant methodologies differ significantly from each other. As illustrated in Fig. 8, VTS-PPT divides the slave segment into two virtual segments. Subsequently, it inserts a virtual node, which replaces the role of the existing slave node, at the center of each virtual segment. For each virtual node, a penalty parameter is allocated based on the area of the virtual segment. As shown, local equivalence of the slave surface is achieved because the contact force is applied at the center of each virtual segment. For the local equivalence of the master surface, the VTS-PPT approach projects the area of each virtual segment as well as the virtual node. If the projection of the virtual segment spans multiple master segments, the contact force is distributed according to the ratio of the projection area to the master surface geometry. Otherwise, the contact force is transmitted directly to the master segment. As shown in Fig. 8, each part of the master surface, divided by the existing discretization and projection of the virtual segment, experiences force and moment equivalence.

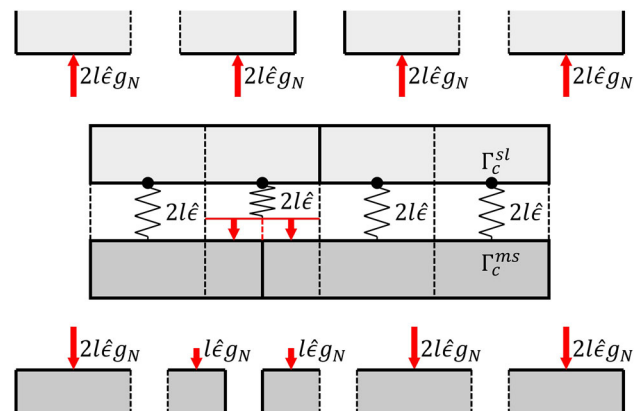


Fig. 8 Patch test of the VTS-PPT approach for uniform penetration: contact force distribution

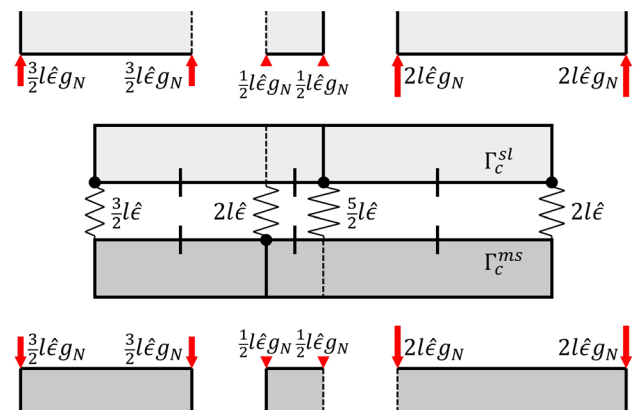


Fig. 9 Patch test of the present NTS-mAR approach for uniform penetration: contact force distribution

Instead of inserting a virtual node, the NTS-mAR approach employs a master node for local equivalence, as illustrated by Fig. 9. First, a contact pair is defined between the slave and master segments, as in the classical one-pass NTS approach. Then, the slave segment in which the nodal projection spans multiple master segments is identified. The master node between these multiple segments is projected onto the identified slave segment, and an additional contact element is created. Penalty parameter regularization is based on a modified competence area, which is the sum of the half-areas obtained from the nearest points between the nodes and projections. Similarly, local equivalence is observed within the segments connecting nodes and projections in the component.

Figure 10 shows that the numerical simulation using the modified NTS approach passes the patch test, regardless of the distributed penalty parameter employed, except for the extremely large value that induces ill conditioning. The modified NTS approach ensures the local equivalence for each contact segment, resulting in uniform penetration as depicted in Fig. 11.

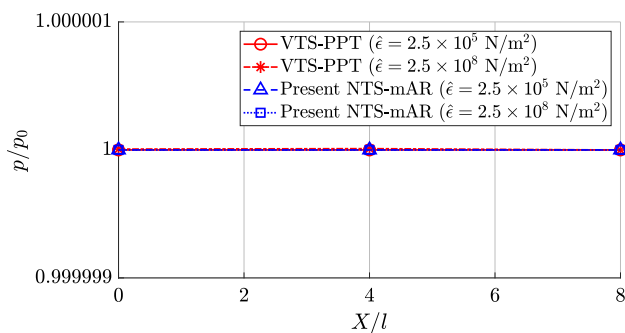


Fig. 10 Patch test of VTS-PPT and the present NTS-mAR approaches via numerical simulation: contact pressure along the slave surface

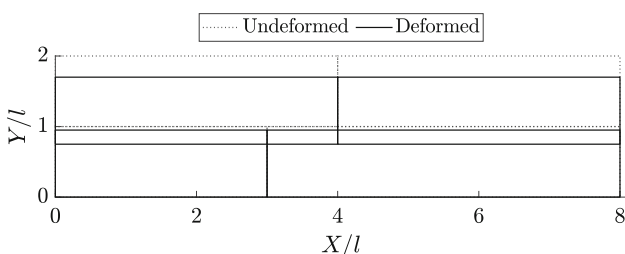


Fig. 11 Patch test of the present NTS-mAR approach via numerical simulation: deformed configuration for $\hat{\epsilon} = 2.5 \times 10^5 \text{ N/m}^2$. Scale factor for the deformation is 5×10^4

3 Computational framework

The accuracy of the modified NTS approach compared with the classical one-pass approach was validated in the previous section and in Refs. [19, 41]. Nevertheless, such accuracy requires additional computations. High computational costs can render modified NTS approaches less competitive than established high-fidelity schemes such as the mortar approach.

It should also be noted that the importance of computational efficiency has increased, particularly for explicit dynamic analysis. For each time step, the conventional explicit solver minimizes the computational cost of the internal force by employing FE with reduced integration [43, 44] and avoids global matrix computation using a lumped mass matrix [45]. Thus, the cost ratio of contact force estimation with respect to the total computation increases. Owing to its efficiency, the classical one-pass penalty-method-based NTS approach remains preferred for simulations using commercial explicit dynamic FE software [8, 9]. Therefore, it is necessary to examine whether the modified NTS approaches enhance accuracy without significantly degrading the computational efficiency in the explicit dynamic framework.

In this section, the computational frameworks of the classical and modified NTS approaches are described. Additionally, the computational setup for the explicit dynamic analysis is explained.

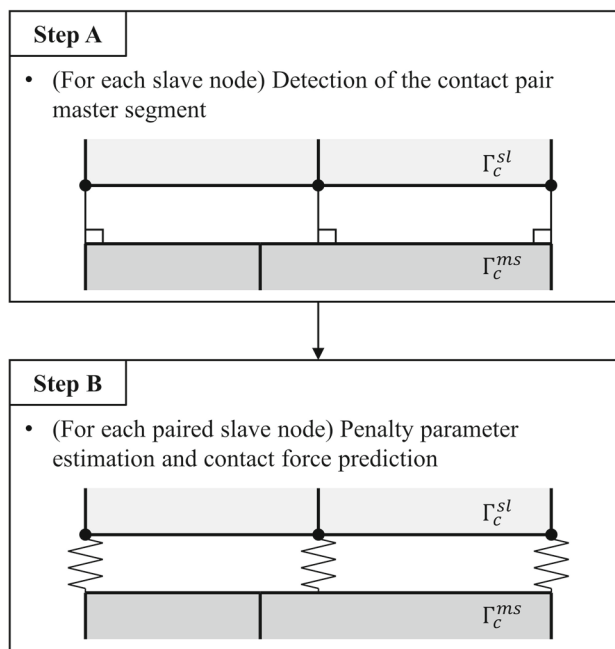


Fig. 12 Computational framework of the classical one-pass NTS approach for contact force prediction

3.1 Algorithm comparison

Figure 12 depicts the computational framework of the classical one-pass NTS approach for contact-force prediction in two steps. In Step A, each slave node detects its contact-pair master segment. In Step B, the contact force for each paired slave node is predicted. With the AR technique, the penalty parameter estimation precedes, the computational cost of which is negligible. Despite its inaccuracy, the classical one-pass NTS approach consists of the simplest framework compared with the VTS-PPT and NTS-mAR approaches.

The computational framework of the VTS-PPT approach is illustrated in Fig. 13. Step A is the same as that in the classical one-pass NTS approach, except that the procedure is conducted for each virtual node. An additional Step M, between Steps A and B, aims to reflect the characteristics of the master surface discretization. The virtual segment related to a paired virtual node is projected onto a master segment. The algorithm then identifies the virtual segment projected onto multiple master segments for further contact-force distribution. In Step B, the penalty parameter for each paired virtual node is estimated based on the area of the virtual segment. Subsequently, the contact force is predicted. The contact force distribution is determined if the virtual segment projection is associated with multiple master segments.

There are N_n^{sl} slave and $2N_n^{sl} - 2$ virtual nodes if $N_n^{sl} - 1$ slave segments are adjoining. This implies that the computational cost of Step A in the VTS-PPT approach is approximately twice that of the classical one-pass NTS

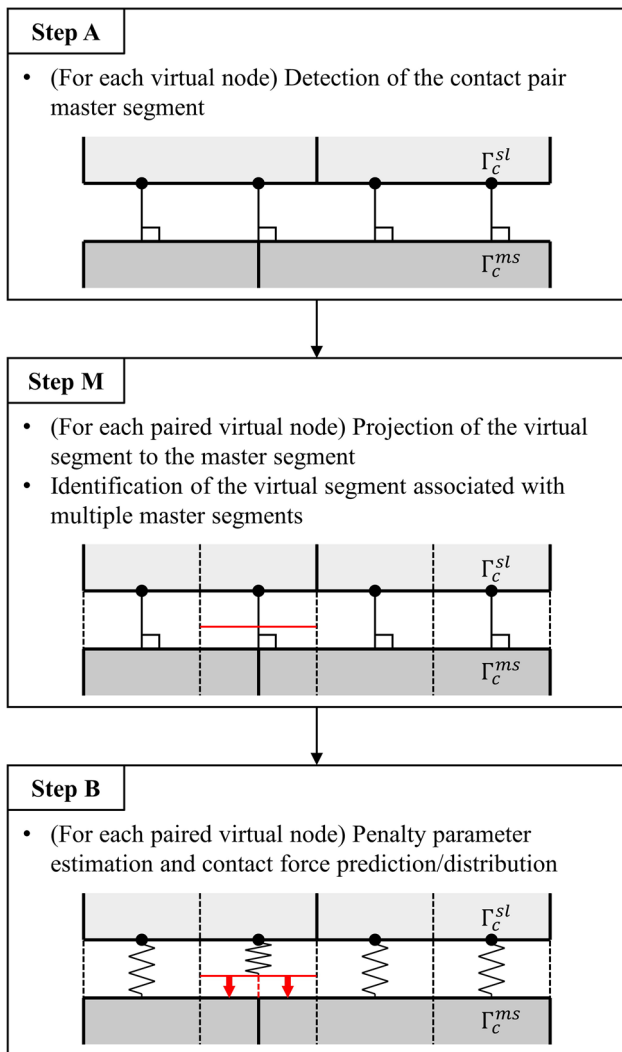


Fig. 13 Computational framework of VTS-PPT approach for the contact force prediction

approach for a sufficient number of slave segments. The tendency of the cost increase is similar in Step B. Moreover, contact force distribution is required for the virtual node associated with multiple master segments. The computational cost of Step M is expected to be relatively small compared with those of Steps A and B. This is because the virtual segment is projected successively onto the paired master segment and its closest segment, not onto an arbitrary segment.

Figure 14 illustrates the computational framework of the NTS-mAR approach. Step A is identical to that of the classical one-pass NTS approach. Step M identifies the slave segment associated with multiple master segments. Subsequently, the master node between the slave node projections is projected onto the identified slave segment. In Step B, the penalty parameter is estimated based on the modified com-

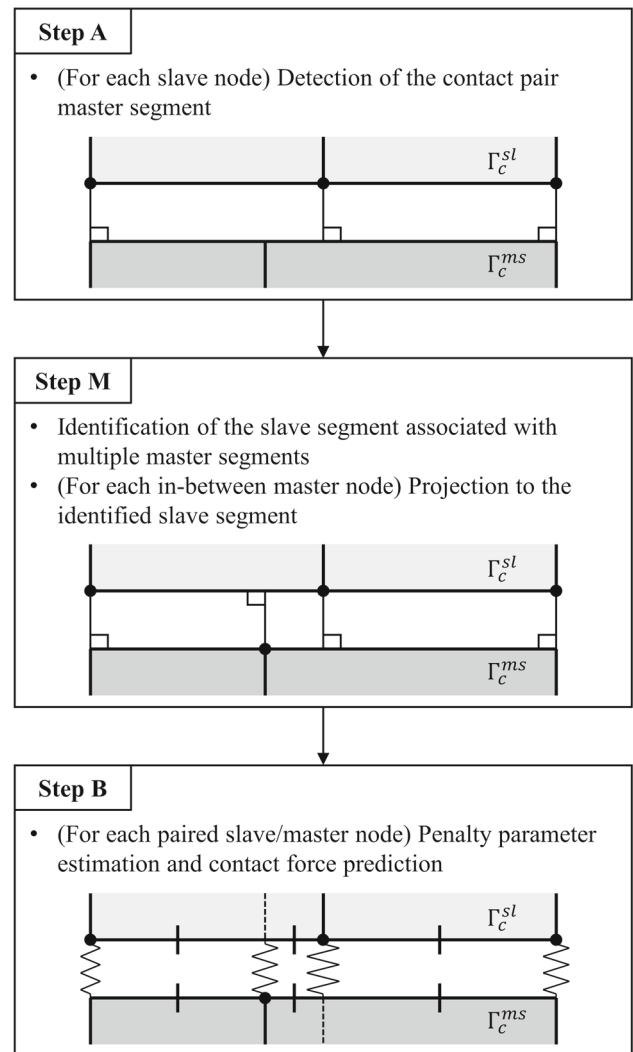


Fig. 14 Computational framework of the present NTS-mAR approach for the contact force prediction

petence area, and the contact force is predicted for both the slave-to-master and master-to-slave contact elements.

In contrast to the VTS-PPT approach, Step A of the NTS-mAR approach is as efficient as that of the classical one-pass NTS approach. The increase in computational cost mainly occurs in Step B owing to the additional master-to-slave contact elements. In a typical situation, the discretization density of the master surface is equal to or lower than that of the slave surface. If there exist \tilde{N}_n^{sl} paired slave nodes for such discretization, a maximum of $\tilde{N}_n^{sl} - 1$ master-to-slave contact elements will be generated. Therefore, the computational cost of the NTS-mAR approach for Step B is approximately twice that of the classical one-pass NTS approach. Similar to the VTS-PPT approach, the computational cost for Step M is expected to be lower than that for Steps A and B. The slave segment associated with multiple master segments can be easily identified by determining whether two end nodes

are projected onto different master segments. Moreover, projection of the in-between master node does not require the detection of the target segment because it is conducted on a pre-identified slave segment.

The NTS-mAR approach, while algorithmically efficient, has a two-pass contact strategy that will potentially lead to an over-constrained scenario, or locking phenomena. As outlined in Ref. [41], employing a partial two-pass contact strategy for the selected master-to-slave elements will mitigate the locking phenomena, except when faced with an exceptionally large penalty parameter value. However, the NTS-mAR method is not entirely free from locking, as it will eventually experience such phenomenon for increased penalty parameter values. Consequently, it is not theoretically feasible to develop an equivalent Lagrange-multiplier-based scheme. This will become required in an explicit analysis when the penalty-method-based contact strategy demands a large penalty parameter to maintain an acceptable penetration and subsequently results in a significantly reduced time step size.

3.2 Computational setup

Herein, the computational setup for the explicit dynamic analysis is introduced. The central differencing method is employed for explicit time integration [46]. The internal force was calculated using the quadrilateral FE of a one-point integration scheme with a viscous hourglass control [43]. The stress update was based on the equation of state and Jaumann stress rate, under the assumption of plane strain. For elastoplastic materials, perfect plasticity is assumed in the plastic regime after the yield strength is reached. A detailed explanation on the stress update and elastoplastic materials employed is provided in Appendix A. A lumped mass matrix was used to efficiently update the acceleration [45], and the damping matrix is neglected.

Before combining the contact approaches validated in a previous patch test and in Ref. [41], the present explicit dynamic framework is validated using an example that does not involve contact interactions, as shown in Fig. 15. This example was based on a previous study [43], and the elastoplastic material property was additionally employed. An upward vertical load was applied to the symmetrical pinned plate. The half-configuration was discretized using 8×4 quadrilateral FEs. Material properties of $E = 1 \text{ GPa}$, $\nu = 0.3$, and $\rho = 1000 \text{ kg/m}^3$ were assigned, where ρ indicates the density.

Figure 16 shows the vertical displacement u_y with respect to time t . Excellent agreement between the present prediction and that of the commercial FE software LS-DYNA [8] was observed for both elastic and elastoplastic materials, indicating that the present explicit dynamic framework

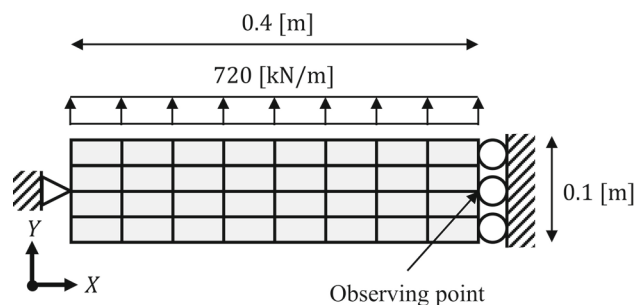


Fig. 15 Schematic of the symmetric plate

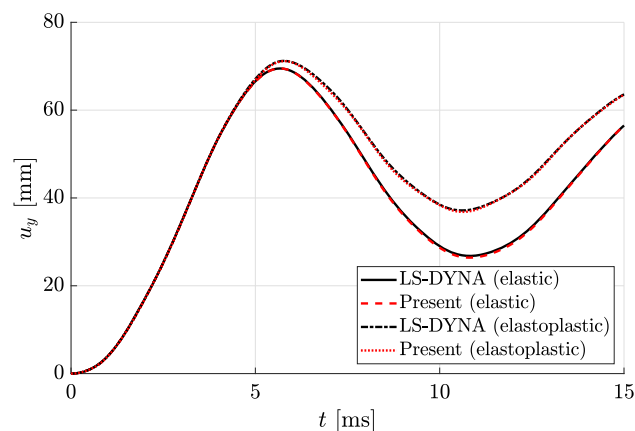


Fig. 16 Symmetric plate: vertical displacement of the observing point according to the time integration

was successfully constructed to be combined with contact approaches.

4 Results and discussions

In this section, the contact approaches are implemented in an explicit dynamic framework and compared using various examples with an emphasis on computational efficiency. An analysis using the penalty-method-based mortar approach [30] was performed for each example. Furthermore, the fully two-pass NTS-AR approach [19, 23, 41] was studied, recognizing that the two-pass NTS method with variable penalty weighting, as found in LS-DYNA, is among the methods prevalently utilized in the industry. For the classical one-pass NTS approach with a penalty parameter of $\epsilon = \epsilon_{\text{NTS}}$, the distributed penalty parameter $\hat{\epsilon}$ was employed as $\epsilon_{\text{NTS}}/l^{sl}$ for the VTS-PPT, NTS-mAR, and mortar approaches, where l^{sl} denotes the average slave segment area. The distributed penalty parameter $\hat{\epsilon}$ of the two-pass NTS-AR approach was selected to be $\epsilon_{\text{NTS}}/l^{sl}$ and $\epsilon_{\text{NTS}}/l^{ms}$ for the slave and master surfaces, respectively. Herein, l^{ms} is the average master segment area. For the example of sliding contact and collision analysis in Sects. 4.2 and 4.3, a refinement study was

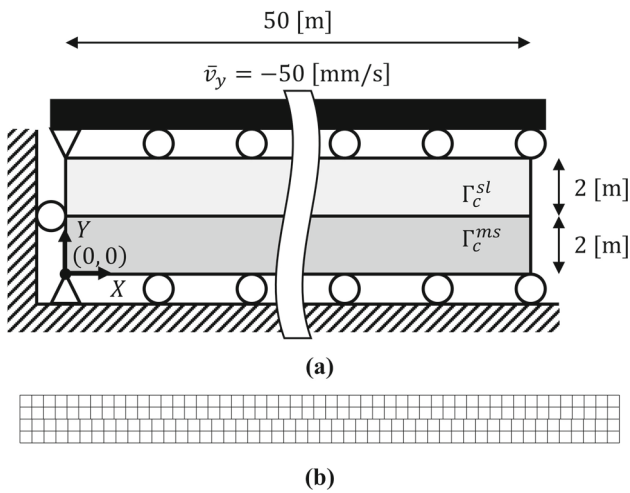


Fig. 17 Block-to-block contact: a schematic and b discretization

conducted for an efficiency comparison in various sets of discretization. As refinement level N_r increases, the mesh size decreases. The time step size also decreases to retain the numerical stability of the explicit analysis. The simulation was conducted on a MATLAB R2021a implementation with a single processor of Intel i9-10900KF 3.70 GHz CPU.

4.1 Block-to-block contact

Figure 17 illustrates an example of block-to-block contact, which is similar to that of the previous patch test shown in Fig. 4, except that dynamic analysis is performed herein. In addition, a vertical speed of $\bar{v}_y = -50$ mm/s was prescribed on the top of the upper block instead of the distributed pressure. The rectangular blocks were replaced with configurations with higher aspect ratios. The slave and master bodies were discretized using 51×2 and 50×2 quadrilateral FEs. Material properties $E = 1$ MPa, $\nu = 0$, and $\rho = 1000$ kg/m³ were assigned to both the slave and master bodies. A penalty parameter of $\epsilon = 1$ MN/m was used in the classical one-pass NTS approach. Time integration was conducted through 200 steps with a step size of $\Delta t = 1$ ms. For the mortar approach, a four-point Gaussian integration rule was used for each slave segment.

In addition to comparing the contact approaches, the cost ratio of the contact algorithm with respect to the total computation between the implicit and explicit analyses was compared. Implicit analysis uses a consistent mass matrix and a fully integrated FE. Additionally, it employs the generalized α method [47] with an energy convergence criterion of $\Delta \mathbf{U}^T \mathbf{R} / \Delta \mathbf{U}_0^T \mathbf{R}_0 < 10^{-20}$ for each Newton–Raphson iteration. Herein, $\Delta \mathbf{U}$ and \mathbf{R} are the global displacement increment and residual force vectors, respectively. Those obtained from the initial Newton–Raphson iteration of each time integration are denoted as $\Delta \mathbf{U}_0$ and \mathbf{R}_0 . Validation of the

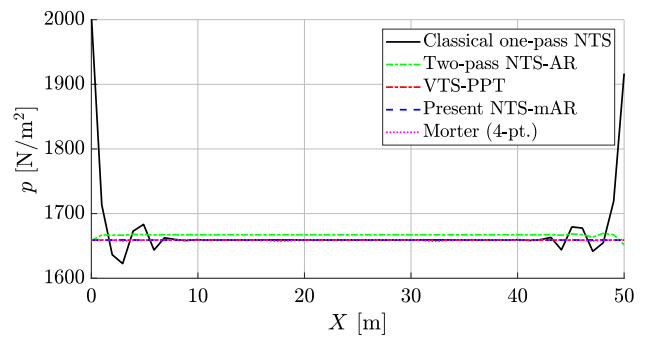


Fig. 18 Block-to-block contact by the implicit dynamic analysis framework: contact pressure along the slave surface at $t = 0.2$ s

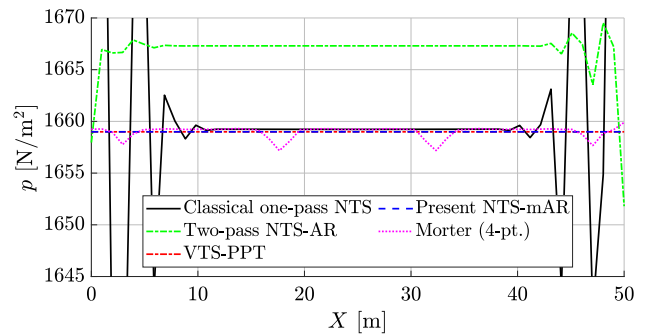


Fig. 19 Block-to-block contact by the implicit dynamic analysis framework: contact pressure along the slave surface at $t = 0.2$ s (Enlarged view)

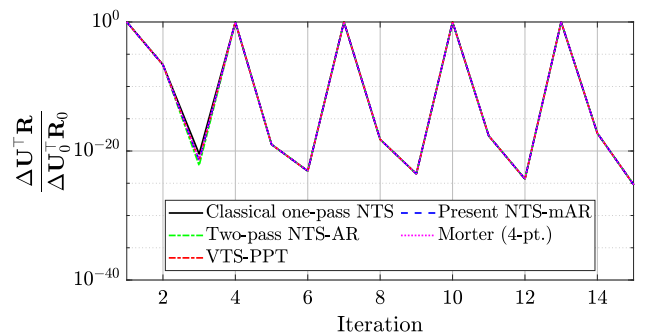


Fig. 20 Block-to-block contact by the implicit dynamic analysis framework: convergence history for the first 5 time steps

present implicit time integration with commercial software can be found in Ref. [48].

Figures 18 and 19 shows the contact-pressure distribution predicted using an implicit analysis framework. The classical one-pass NTS approach displayed an anomalously large contact pressure at the termination of contact surface. Despite the failure in passing the patch test, the two-pass NTS-AR method mitigated such nonuniformity. However, the contact pressure decreased at the end of contact surface. Refs. [19, 41] observed a similar trend during the contact patch test with uniform surface discretization. Apart from those two approaches, the mortar approach predicted relatively uniform

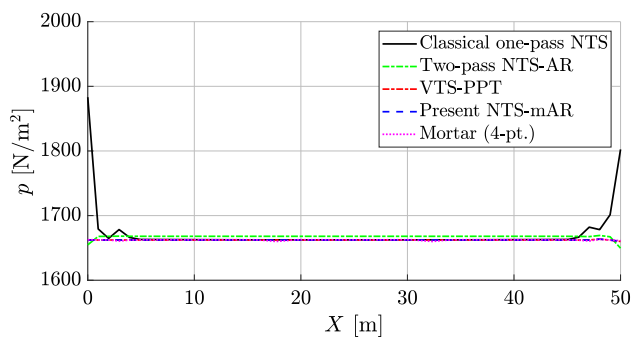


Fig. 21 Block-to-block contact by the explicit dynamic analysis framework: contact pressure along the slave surface at $t = 0.2$ s

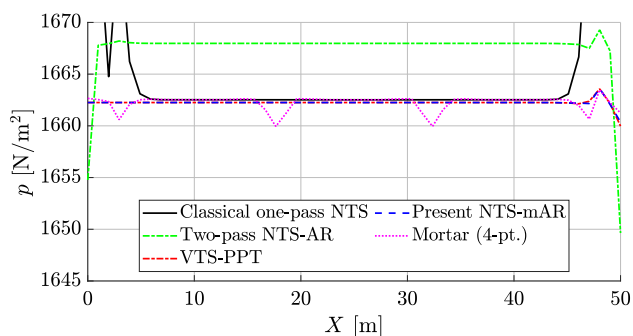


Fig. 22 Block-to-block contact by the explicit dynamic analysis framework: contact pressure along the slave surface at $t = 0.2$ s (Enlarged view)

contact pressure, and the VTS-PPT and present NTS-mAR approaches exhibited perfectly uniform pressure. The energy convergence criterion was satisfied within three Newton–Raphson iterations for most time steps, as shown in Fig. 20. Such a small number of iterations is due to the situation of small deformation and the relatively small time step size for the implicit analysis. The prediction using the explicit analysis framework is shown in Figs. 21 and 22, where the tendency of the uniformity is similar to that in the implicit framework.

Figure 23 compares the computational times for the contact approaches. The time indicated above the blue bar represents the computational time required for the contact contribution. The ratio in parentheses denotes the cost ratio of the contact contribution with respect to the total computation. As expected, the classical one-pass NTS approach exhibited the highest computational speed. Except this, the NTS-mAR approach was the most efficient. The two-pass NTS-AR method required approximately double the computational time compared against the classical one-pass approach. Such increase is attributed to the added contact force estimation for the master-to-slave elements, which are nearly equal in number to the slave-to-master elements. The computational time for the VTS-PPT was thrice that for the classical one-pass NTS approach, and even close to that of the mortar

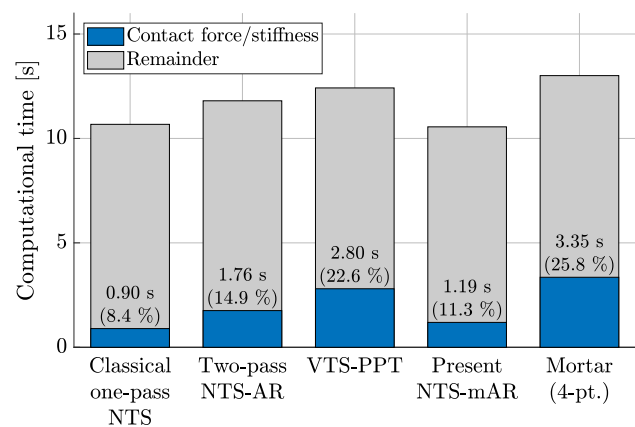


Fig. 23 Block-to-block contact by the implicit dynamic analysis framework: computational time. (Color figure online)

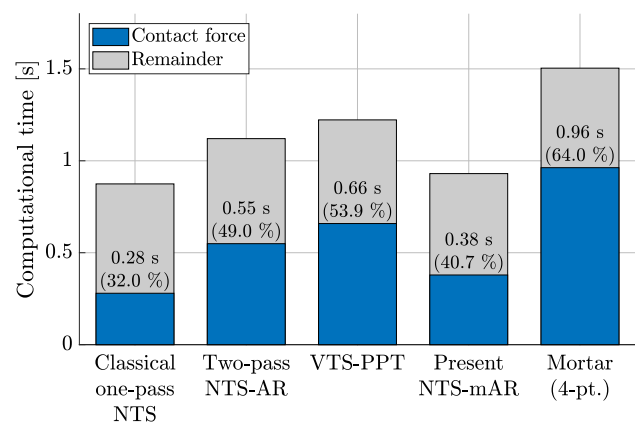


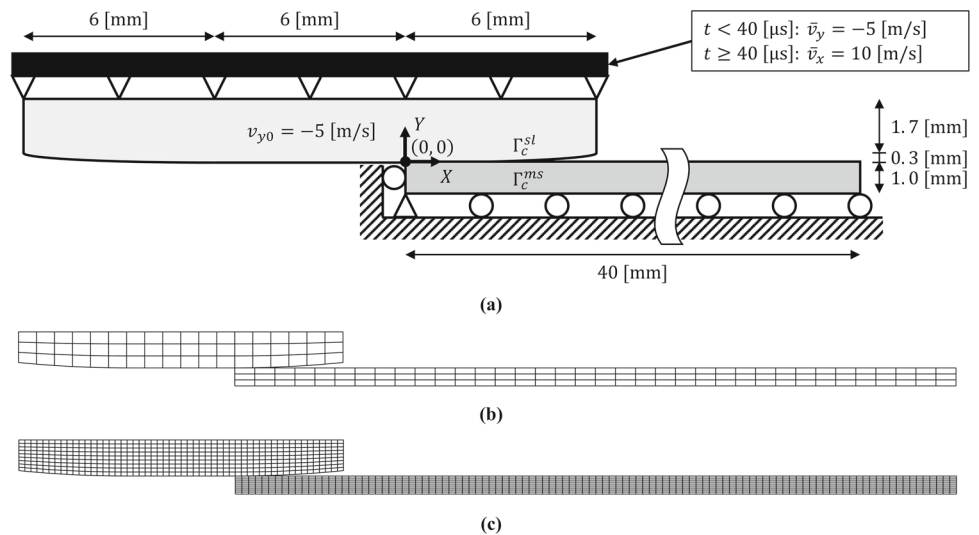
Fig. 24 Block-to-block contact by the explicit dynamic analysis framework: computational time

approach. This may be due to the relatively complicated calculation of contact stiffness [19]. Similarly, in the explicit framework, the NTS-mAR approach was the fastest, excluding the classical one-pass NTS approach, as shown in Fig. 24. The computational cost of the VTS-PPT approach, which is alleviated because of the absence of contact stiffness computation, was 2.4 times that of the classical one-pass NTS approach. The overall cost ratio of the contact contribution with respect to the total computation increased in the explicit dynamic framework.

4.2 Sliding contact

Figure 25 illustrates an example of sliding contact condition, for which the situation is taken from Refs. [31, 49]. The elastic die initially moved downward to press the elasto-plastic plate and then moved horizontally. The die and plate, which were designated as the slave and master bodies, were discretized by $18N_r \times 3N_r$ and $36N_r \times 4N_r$ quadrilateral FEs, respectively. The material properties $E = 210$ GPa,

Fig. 25 Sliding contact: **a** schematic, discretization for **b** $N_r = 1$ and **c** $N_r = 3$



$\nu = 0.3$, and $\rho = 7,850 \text{ kg/m}^3$ were assigned to the die, and $E = 69 \text{ GPa}$, $\nu = 0.33$, $\rho = 2700 \text{ kg/m}^3$, and $\sigma^Y = 276 \text{ MPa}$ were assigned to the plate. Here, σ^Y is the yield strength. A penalty parameter of $\epsilon = \epsilon_{\text{NTS}}^1 / N_r$, where $\epsilon_{\text{NTS}}^1 = 10 \text{ GN/m}$, was used in the classical one-pass NTS approach. Explicit time integration was conducted using $150,000 N_r$ steps with a step size of $\Delta t = \Delta t^1 / N_r$, where $\Delta t^1 = 40 \text{ ns}$. A six-point Gaussian integration rule was employed for each slave segment in the mortar approach.

A snapshot of the deformation and effective plastic strain is shown in Fig. 26. The classical one-pass NTS approach slightly overestimated the effective plastic strain at $X = 0$ owing to the local peak of the contact pressure. In contrast, the two-pass NTS-AR approach underestimated the contact pressure at $X = 0$, and leading to an overestimation of the contact pressure and the subsequent deformation in the remaining regions. Such inaccuracy is unavoidable in the contact approach that does not pass the patch test. The sum of the vertical contact forces applied to the slab is shown in Figs. 27 and 28 in terms of time. The classical one-pass NTS approach suffers from nonphysical oscillations with high amplitudes. The abrupt peak of the contact force was due to the activation and deactivation of the contact element. As is well known [31], the mortar approach significantly reduces such oscillations and exhibits the most uniform contact force history. The overall force magnitude of the VTS-PPT and the present NTS-mAR approaches was approximated as that of the mortar approach. Comparing the modified NTS approaches passing the patch test, NTS-mAR predicted a smoother contact force history than the VTS-PPT approach. Moreover, the NTS-mAR approach predicted the lowest number of abrupt peaks owing to the complementary action between the slave-to-master and master-to-slave contact pairs. Nevertheless, once the peak occurred, its mag-

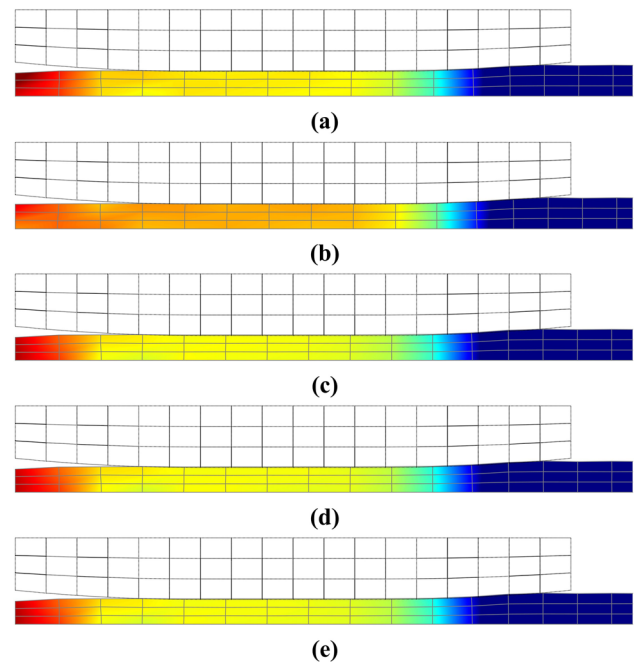


Fig. 26 Sliding contact with $N_r = 1$: distribution of the effective plastic strain at $t = 12.4 \text{ ms}$ predicted by **a** classical one-pass NTS, **b** two-pass NTS-AR, **c** VTS-PPT, **d** present NTS-mAR, and **e** mortar approaches. The colormap ranges from 0.1 to 0.3. (Color figure online)

nitude was larger than those of the two-pass NTS, VTS-PPT, and mortar approaches.

The computation times are compared in Fig. 29. The two-pass NTS-AR and VTS-PPT approaches requires more than twice the computational cost for the contact force estimation than the classical one-pass NTS approach. In contrast, NTS-mAR requires only 22% additional time compared to the classical one-pass NTS approach. Such tendency of the cost is maintained even if the refinement level increases as shown in Table 1. Thus, the NTS-mAR approach is better when a

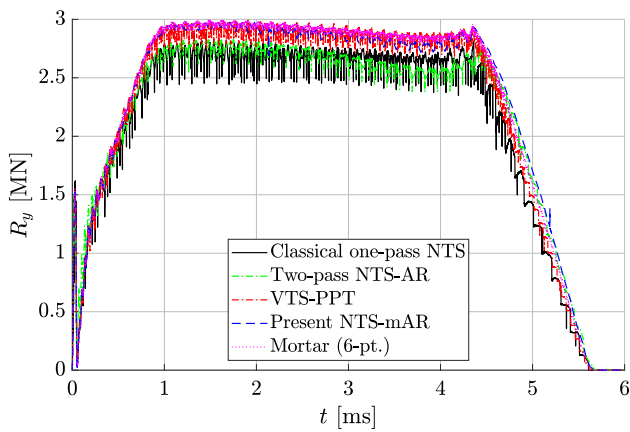


Fig. 27 Sliding contact with $N_r = 1$: total vertical contact force applied on the slab according to the time integration

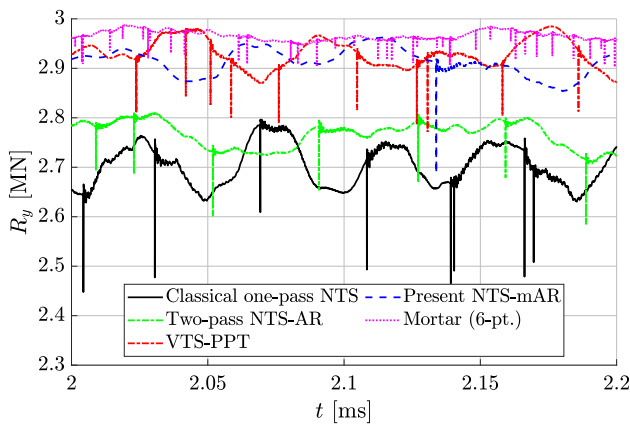


Fig. 28 Sliding contact with $N_r = 1$: total vertical contact force applied on the slab according to the time integration (Enlarged view)

computational efficiency with mid-fidelity is desired for the given example.

4.3 Collision analysis

Figure 30 illustrates the attempted collision analysis. The high-speed elastic projectile initially moved downward and collided with the elastoplastic plate. The projectile and plate were designated as the slave and master bodies, respectively,

Table 1 Sliding contact: computational time for contact force estimation according to the refinement level

	Time (s)		
	$N_r = 1$	$N_r = 2$	$N_r = 3$
Classical one-pass NTS	62 (1.00)	451 (1.00)	1446 (1.00)
Two-pass NTS-AR	140 (2.25)	1020 (2.26)	3269 (2.26)
VTS-PPT	130 (2.09)	941 (2.09)	3177 (2.20)
Present NTS-mAR	76 (1.22)	493 (1.09)	1623 (1.12)
Mortar (6-pt.)	310 (4.98)	2474 (5.49)	8462 (5.85)

The values between the parenthesis indicate the cost ratio to the classical one-pass NTS approach

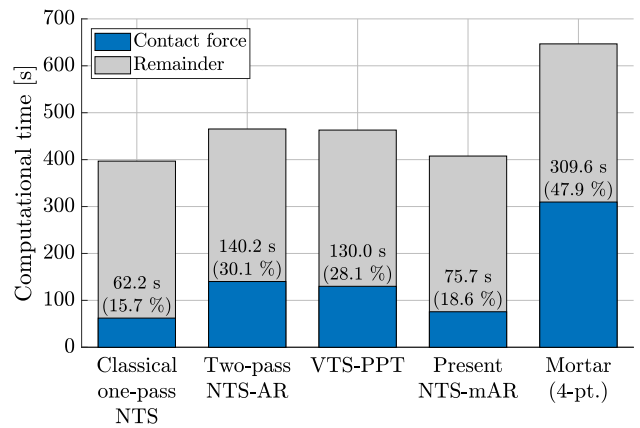


Fig. 29 Sliding contact with $N_r = 1$: computational time

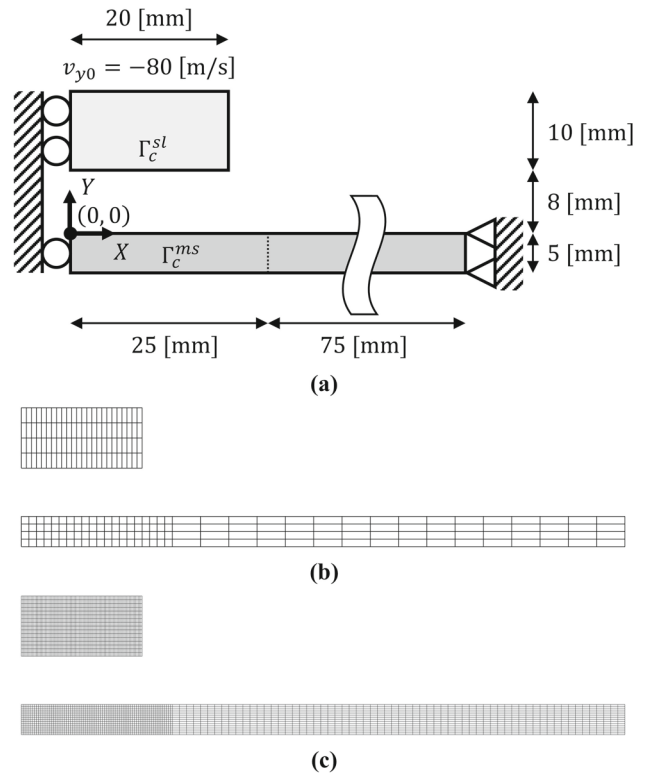


Fig. 30 Collision analysis: **a** schematic, discretization for **b** $N_r = 1$ and **c** $N_r = 4$

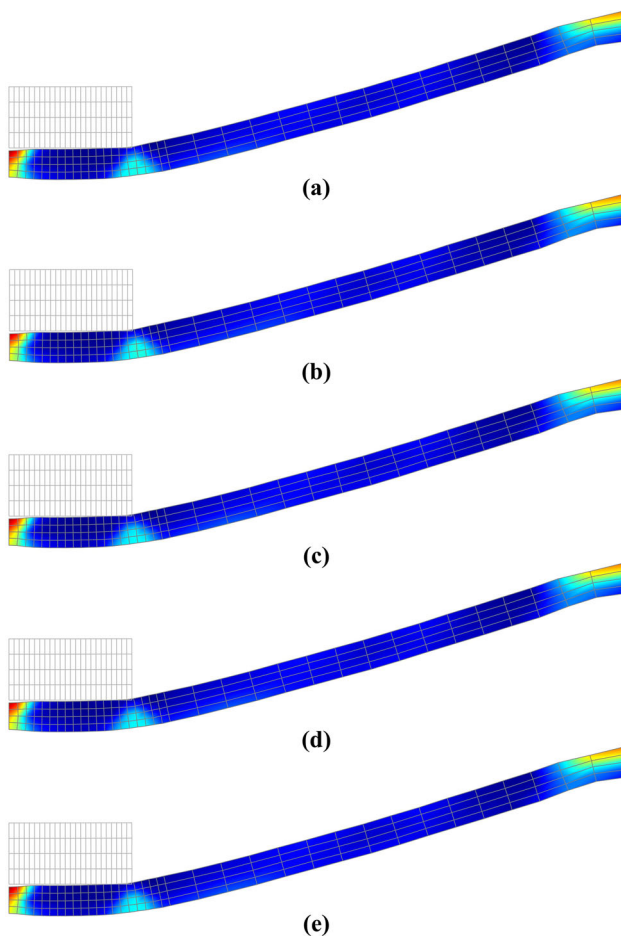


Fig. 31 Collision analysis with $N_r = 1$: distribution of the effective plastic strain at $t = 0.7$ ms predicted by **a** classical one-pass NTS, **b** two-pass NTS-AR, **c** VTS-PPT, **d** present NTS-mAR, and **e** mortar approaches. The colormap ranges from 0 to 0.25. (Color figure online)

and were discretized using $24N_r \times 4N_r$ and $36N_r \times 4N_r$ quadrilateral FEs. For the master body, relatively fine discretization of $20N_r \times 4N_r$ constituted the region of $X \leq 25$ mm, where the master surface was designated. The properties of the elastic and elastoplastic materials were the same as those in the above-mentioned example. A penalty parameter of $\epsilon = \epsilon_{\text{NTS}}^1/N_r$, where $\epsilon_{\text{NTS}}^1 = 1$ GN/m, was used in the classical one-pass NTS approach. Explicit time integra-

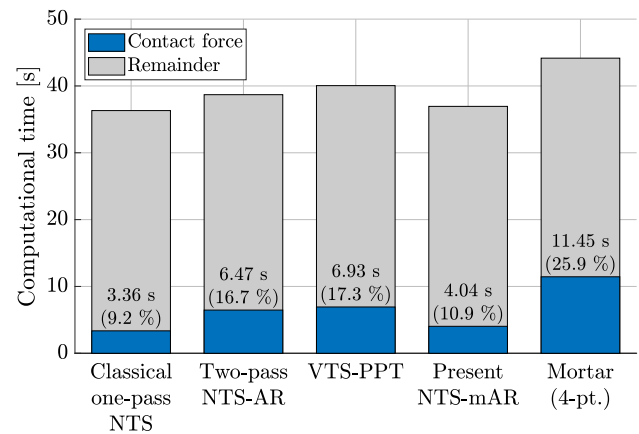


Fig. 32 Collision analysis with $N_r = 1$: computational time

tion was conducted using $10,000N_r$ steps with a step size of $\Delta t = \Delta t^1/N_r$, where $\Delta t^1 = 100$ ns. A four-point Gaussian integration rule was employed for the mortar approach.

Figure 31 shows the deformation and effective plastic strain. Except for a slight overestimation in the bent regime by the classical one-pass NTS approach, all approaches predicted almost identical results. In contrast to the previous examples, the duration of contact occurrence is relatively small compared to the total physical duration because the two bodies repeatedly attach to and detach from each other. This is one of the possible reasons why different selections of the contact approach did not provide a significant difference in the prediction.

Nevertheless, the computational time for contact force estimation shows a significant difference among the contact approaches, as illustrated in Fig. 32. Furthermore, such a difference is maintained for the refined mesh and time step size, as shown in Table 2. This is because the detection procedure (Step A in Sect. 3.1) occurs even for the instance of no contact interaction. The total computational time might increase if a relatively large portion is assigned as the slave surface. Including the current example, NTS-mAR required the least additional computational cost to alter the classical one-pass NTS approach.

Table 2 Collision analysis: computational time for contact force estimation according to the refinement level

	Time (s)			
	$N_r = 1$	$N_r = 2$	$N_r = 3$	$N_r = 4$
Classical one-pass NTS	3 (1.00)	23 (1.00)	74 (1.00)	170 (1.00)
Two-pass NTS-AR	6 (1.92)	45 (1.97)	143 (1.95)	328 (1.93)
VTS-PPT	7 (2.06)	46 (2.05)	150 (2.04)	348 (2.05)
Present NTS-mAR	4 (1.20)	25 (1.09)	78 (1.06)	179 (1.06)
Mortar (4-pt.)	11 (3.41)	85 (3.76)	281 (3.82)	642 (3.78)

The values between the parenthesis indicate the cost ratio to the classical one-pass NTS approach

5 Conclusions

This study examined the computational procedure of modified penalty-method-based NTS approaches, the accuracy improvement of which against the classical approach was emphasized in the implicit static context only. These are extended to an explicit dynamic framework in which the cost ratio of contact estimation with respect to the total computation is larger than that in implicit analysis. A quantitative performance comparison was conducted, and the following conclusions were drawn.

- As expected, the classical one-pass NTS approach is the fastest contact analysis approach for the given examples despite its inaccuracy.
- Excluding that, the NTS-mAR approach is the most efficient modified NTS approach and provides relatively accurate prediction compared with the classical one-pass NTS approach.
- The accuracy is found to be similar between VTS-PPT and NTS-mAR approaches for the given examples.
- For the sliding contact, an abrupt peak of the contact force occurs owing to the deactivation and activation of the contact element. The number of the peaks is reduced by the complementary action of the dual-pass algorithm in NTS-mAR approach.
- The mortar approach provides the most uniform contact force history for the sliding contact. However, its computational cost is significant.
- For the relatively short duration of the contact interaction, the efficiencies of the classical one-pass NTS and NTS-mAR approaches are valid owing to the detection stage prevailing in the total duration.

Thus, for the given examples, the NTS-mAR approach is the most appropriate when computational efficiency with mid-fidelity is desired.

The competitiveness of the NTS-mAR approach will dramatically improve when it is extended to the three-dimensional analysis. Relevant techniques are currently being examined to consider an arbitrary master surface geometry and pass the patch test in a three-dimensional condition.

Acknowledgements The authors would like to acknowledge the financial support provided by the Defense Rapid Acquisition Technology Research Institute (DRATRI) of Korea (Project Code 912849501).

Declarations

Conflict of interest The authors declare no conflict of interest.

Open Access This article is licensed under a Creative Commons Attribution 4.0 International License, which permits use, sharing, adaptation, distribution and reproduction in any medium or format, as long as you give appropriate credit to the original author(s) and the

source, provide a link to the Creative Commons licence, and indicate if changes were made. The images or other third party material in this article are included in the article's Creative Commons licence, unless indicated otherwise in a credit line to the material. If material is not included in the article's Creative Commons licence and your intended use is not permitted by statutory regulation or exceeds the permitted use, you will need to obtain permission directly from the copyright holder. To view a copy of this licence, visit <http://creativecommons.org/licenses/by/4.0/>.

Appendix A: Stress update and elastoplastic material

This section explains the computational procedure for the stress update and elastoplastic material employed in the present explicit dynamic analysis framework. A theoretical background can be found in Refs. [8, 50, 51].

The update of volumetric stress tensor σ_{vol} for isotropic material is based on the equation of state as in Eq. (A1).

$$\sigma_{vol} = -K \ln(J)\mathbf{I} \tag{A1}$$

Herein, K is the bulk modulus, and J is the determinant of the deformation gradient, which is the volume ratio between current and initial configurations.

For the update of deviatoric stress tensor σ_{dev} , the Jaumann stress rate of hypoealstic material law is used. For it, deformation rate tensor \mathbf{D} and spin tensor \mathbf{W} at each integration point are obtained as in Eqs. (A2) and (A3).

$$\mathbf{D} = \frac{1}{2} \left((\nabla \mathbf{v})^\top + (\nabla \mathbf{v}) \right) \tag{A2}$$

$$\mathbf{W} = \frac{1}{2} \left((\nabla \mathbf{v})^\top - (\nabla \mathbf{v}) \right) \tag{A3}$$

Herein, $\nabla \mathbf{v}$ is the velocity gradient.

Then, the trial deviatoric Cauchy stress tensor σ_{dev}^* is obtained under the elastic assumption as in Eq. (A4).

$$\sigma_{dev}^* = \sigma_{dev}^{old} + \left(\sigma_{dev}^{\nabla J} + \mathbf{W} \cdot \sigma_{dev}^{old} + \sigma_{dev}^{old} \cdot \mathbf{W}^\top \right) \Delta t \tag{A4}$$

Deviatoric stress tensor obtained from the previous time step is denoted as σ_{dev}^{old} . Furthermore, $\sigma_{dev}^{\nabla J}$ is the Jaumann stress rate of the deviatoric part, which is calculated as $\sigma^{\nabla J} = 2G\mathbf{D}_{dev}$ for the isotropic material. Herein, G is the shear modulus and \mathbf{D}_{dev} is the deviatoric part of \mathbf{D} .

To consider the elastoplasticity, the yield criterion is evaluated as $\phi = \sigma_v^* - \sigma^Y$, where σ_v^* is the trial von-Mises stress obtained from σ_{dev}^* . Herein, yield strength σ^Y is constant according to the perfect plasticity employed. If $\phi \leq 0$, the deviatoric stress tensor becomes $\sigma_{dev} = \sigma_{dev}^*$. If $\phi > 0$, it is

scaled back as in Eq. (A5).

$$\sigma_{\text{dev}} = \frac{\sigma^Y}{\sigma_v^*} \sigma_{\text{dev}}^* \quad (\text{A5})$$

For $\phi > 0$, the effective plastic strain increment $\Delta \bar{\epsilon}$ is obtained as Eq. (A6).

$$\Delta \bar{\epsilon} = \frac{\phi}{3G + E_p} \quad (\text{A6})$$

Herein, E_p is the plastic hardening modulus which is $E_p = 0$ for perfect plasticity.

References

- Hughes TJR, Taylor RL, Sackman JL, Curmire A, Kanoknukulchai W (1976) A finite element method for a class of contact-impact problems. *Comput Methods Appl Mech Eng* 8(3):249–276. [https://doi.org/10.1016/0045-7825\(76\)90018-9](https://doi.org/10.1016/0045-7825(76)90018-9)
- Hughes TJR, Taylor RL, Kanoknukulchai W (1977) A finite element method for large displacement contact and impact problems. In: Bathe KJ, Oden JT, Wunderlich W (eds) *Formulations and computational algorithms in finite element analysis*. MIT Press, Boston, pp 468–495
- Hallquist JO (1979) NIKE2D: an implicit, finite deformation, finite element code for analyzing the static and dynamic response of two dimensional solids. Technical Report UCRL-52678, Lawrence Livermore National Laboratory, California University, Livermore
- Hallquist JO, Goudreau GL, Benson DJ (1985) Sliding interfaces with contact-impact in large-scale Lagrangian computations. *Comput Methods Appl Mech Eng* 51(1–3):107–137. [https://doi.org/10.1016/0045-7825\(85\)90030-1](https://doi.org/10.1016/0045-7825(85)90030-1)
- Zavarise G, De Lorenzis L (2009) The node-to-segment algorithm for 2D frictionless contact: classical formulation and special cases. *Comput Methods Appl Mech Eng* 198(41–44):3428–3451. <https://doi.org/10.1016/j.cma.2009.06.022>
- Wriggers P (2006) *Computational contact mechanics*, 2nd edn. Springer, Berlin
- Konyukhov A, Izi R (2015) *Introduction to computational contact mechanics: a geometrical approach*. John Wiley & Sons, Chichester
- Anonymous (2017) LS-DYNA Theory Manual; Release 10.0. Livermore Software Technology Corporation, Livermore
- Anonymous (2022) Altair Radioss 2022 Theory Manual. Altair Engineering Inc., Troy
- Taylor RL, Papadopoulos P (1991) On a patch test for contact problems in two dimensions. In: Wriggers P, Wagner W (eds) *Nonlinear computational mechanics*. Springer, Berlin, pp 690–702
- Crisfield MA (2000) Re-visiting the contact patch test. *Int J Numer Methods Eng* 48(3):435–449. [https://doi.org/10.1002/\(SICI\)1097-0207\(20000530\)48:3<435::AID-NME891>3.0.CO;2-V](https://doi.org/10.1002/(SICI)1097-0207(20000530)48:3<435::AID-NME891>3.0.CO;2-V)
- El-Abbasi N, Bathe KJ (2001) Stability and patch test performance of contact discretizations and a new solution algorithm. *Comput Struct* 76(16):1473–1486. [https://doi.org/10.1016/S0045-7949\(01\)00048-7](https://doi.org/10.1016/S0045-7949(01)00048-7)
- Park KC, Felippa CA, Rebel G (2002) A simple algorithm for localized construction of non-matching structural interfaces. *Int J Numer Methods Eng* 53(9):2117–2142. <https://doi.org/10.1002/nme.374>
- Tan D (2003) Mesh matching and contact patch test. *Comput Mech* 31:135–152. <https://doi.org/10.1007/s00466-002-0400-5>
- Kim JH, Lim JH, Lee JH, Im S (2008) A new computational approach to contact mechanics using variable-node finite elements. *Int J Numer Methods Eng* 73(13):1966–1988. <https://doi.org/10.1002/nme.2162>
- Jin S, Sohn D, Lim JH, Im S (2015) A node-to-node scheme with the aid of variable-node elements for elasto-plastic contact analysis. *Int J Numer Methods Eng* 102(12):1761–1783. <https://doi.org/10.1002/nme.4862>
- Jin S, Sohn D, Im S (2016) Node-to-node scheme for three-dimensional contact mechanics using polyhedral type variable-node elements. *Comput Methods Appl Mech Eng* 304:217–242. <https://doi.org/10.1016/j.cma.2016.02.019>
- Zavarise G, Wriggers P, Stein E, Schrefler BA (1992) Real contact mechanisms and finite element formulation—a coupled thermo-mechanical approach. *Int J Numer Methods Eng* 35(4):767–785. <https://doi.org/10.1002/nme.1620350409>
- Zavarise G, De Lorenzis L (2009) A modified node-to-segment algorithm passing the contact patch test. *Int J Numer Methods Eng* 79(4):379–416. <https://doi.org/10.1002/nme.2559>
- Lee SM (2022) Improved contact and collision analysis by using three-dimensional node-to-segment area regularization. Master's thesis, Seoul National University, Seoul
- Lee SM, Kang SH, Shin SJ (2022) Three-dimensional contact analysis for a stiffened plate panel using the node-to-segment area regularization. In: *Proceedings of AIAA SciTech 2022 Forum*, San Diego, p 2268. <https://doi.org/10.2514/6.2022-2268>
- Kwon SL, Lee S, Ha D, Yun GJ (2023) A fully nonlinear three-dimensional dynamic frictional contact analysis method under large deformation with the area regularization. *Eng Comput*. <https://doi.org/10.1007/s00366-023-01795-x>
- Anonymous (2017) LS-DYNA Keyword User's Manual; Release 10.0 vol. 1. Livermore Software Technology Corporation, Livermore
- Simo JC, Wriggers P, Taylor RL (1985) A perturbed Lagrangian formulation for the finite element solution of contact problems. *Comput Methods Appl Mech Eng* 50(2):163–180. [https://doi.org/10.1016/0045-7825\(85\)90088-X](https://doi.org/10.1016/0045-7825(85)90088-X)
- Papadopoulos P, Taylor RL (1992) A mixed formulation for the finite element solution of contact problems. *Comput Methods Appl Mech Eng* 94(3):373–389. [https://doi.org/10.1016/0045-7825\(92\)90061-N](https://doi.org/10.1016/0045-7825(92)90061-N)
- Zavarise G, Wriggers P (1998) A segment-to-segment contact strategy. *Math Comput Model* 28(4–8):497–515. [https://doi.org/10.1016/S0895-7177\(98\)00138-1](https://doi.org/10.1016/S0895-7177(98)00138-1)
- Bernardi C, Debit N, Maday Y (1990) Coupling finite element and spectral methods: first results. *Math Comput* 54(189):21–39. <https://doi.org/10.1090/S0025-5718-1990-0995205-7>
- Wohlmuth BI (2000) A mortar finite element method using dual spaces for the Lagrange multiplier. *SIAM J Numer Anal* 38(3):989–1012. <https://doi.org/10.1137/S0036142999350929>
- Puso MA, Laursen TA (2004) A mortar segment-to-segment contact method for large deformation solid mechanics. *Comput Methods Appl Mech Eng* 193(6–8):601–629. <https://doi.org/10.1016/j.cma.2003.10.010>
- Fischer KA, Wriggers P (2005) Frictionless 2D contact formulations for finite deformations based on the mortar method. *Comput Mech* 36:226–244. <https://doi.org/10.1007/s00466-005-0660-y>
- Fischer KA, Wriggers P (2006) Mortar based frictional contact formulation for higher order interpolations using the moving friction cone. *Comput Methods Appl Mech Eng* 195(37–40):5020–5036. <https://doi.org/10.1016/j.cma.2005.09.025>
- Popp A, Gee MW, Wall WA (2009) A finite deformation mortar contact formulation using a primal-dual active set strategy. *Int J Numer Methods Eng* 79(11):1354–1391. <https://doi.org/10.1002/nme.2614>

33. Popp A, Gitterle M, Gee MW, Wall WA (2010) A dual mortar approach for 3D finite deformation contact with consistent linearization. *Int J Numer Methods Eng* 83(11):1428–1465. <https://doi.org/10.1002/nme.2866>
34. Popp A, Wohlmuth BI, Gee MW, Wall WA (2012) Dual quadratic mortar finite element methods for 3D finite deformation contact. *SIAM J Sci Comput* 34(4):421–446. <https://doi.org/10.1137/110848190>
35. De Lorenzis L, Wriggers P, Zavarise G (2012) A mortar formulation for 3D large deformation contact using NURBS-based isogeometric analysis and the augmented Lagrangian method. *Comput Mech* 49:1–20. <https://doi.org/10.1007/s00466-011-0623-4>
36. Puso MA, Solberg JM (2020) A dual pass mortar approach for unbiased constraints and self-contact. *Comput Methods Appl Mech Eng* 367:113092. <https://doi.org/10.1016/j.cma.2020.113092>
37. Anonymous (2012) ABAQUS 6.12 Theory Manual. Dassault Systèmes Simulia Corporation, Providence
38. Wiesner TA, Popp A, Gee MW, Wall WA (2018) Algebraic multigrid methods for dual mortar finite element formulations in contact mechanics. *Int J Numer Methods Eng* 114(4):399–430. <https://doi.org/10.1002/nme.5748>
39. Wiesner TA, Mayr M, Popp A, Gee MW, Wall WA (2021) Algebraic multigrid methods for saddle point systems arising from mortar contact formulations. *Int J Numer Methods Eng* 122(15):3749–3779. <https://doi.org/10.1002/nme.6680>
40. Mayr M, Popp A (2023) Scalable computational kernels for mortar finite element methods. *Eng Comput*. <https://doi.org/10.1007/s00366-022-01779-3>
41. Kang SH, Lee SM, Shin SJ (2023) Improved area regularization technique for penalty-method-based node-to-segment contact analysis. *Comput Mech* 71:801–825. <https://doi.org/10.1007/s00466-023-02269-z>
42. Kang SH, Hwang M, Lee SM, Shin SJ (2023) Elasto-plastic node-to-segment contact analysis based on the improved area regularization technique. In: Proceedings of 2023 KSAS spring conference. The Korean Society for Aeronautical and Space Sciences, Seoul. In Korean, pp 122–123
43. Flanagan DP, Belytschko T (1981) A uniform strain hexahedron and quadrilateral with orthogonal hourglass control. *Int J Numer Methods Eng* 17(5):679–706. <https://doi.org/10.1002/nme.1620170504>
44. Belytschko T, Lin JJ, Tsay CS (1984) Explicit algorithms for the nonlinear dynamics of shells. *Comput Methods Appl Mech Eng* 42(2):225–251. [https://doi.org/10.1016/0045-7825\(84\)90026-4](https://doi.org/10.1016/0045-7825(84)90026-4)
45. Hughes TJR, Liu WK, Levit I (1981) Nonlinear dynamics finite element analysis of shells. In: Wunderlich W, Stein E, Bathe KJ (eds) *Nonlinear finite element analysis in structural mechanics*. Springer, Berlin, pp 151–168
46. Tabiei A, Tanov R (2000) A nonlinear higher order shear deformation shell element for dynamic explicit analysis: Part I. Formulation and finite element equations. *Finite Elem Anal Des* 36(1):17–37. [https://doi.org/10.1016/S0168-874X\(00\)00005-6](https://doi.org/10.1016/S0168-874X(00)00005-6)
47. Chung J, Hulbert GM (1993) A time integration algorithm for structural dynamics with improved numerical dissipation: the generalized- α method. *J Appl Mech* 60(2):371–375. <https://doi.org/10.1115/1.2900803>
48. Kim Y, Kang SH, Cho H, Shin SJ (2022) Improved nonlinear analysis of a propeller blade based on hyper-reduction. *AIAA J* 60(3):1909–1922. <https://doi.org/10.2514/1.J060742>
49. Baillet L, Clair D, Walter H, Brunet M (2000) A 3D contact algorithm for explicit dynamic F.E. codes applied to the ironing process. In: Pietrzyk M, Kusiak J, Majta J, Hartley P, Pillinger I (eds) *Proceedings of the 8th international conference on metal forming*. CRC Press, Boca Raton, pp 141–147
50. Belytschko T, Liu WK, Moran B, Elkhodary KI (2014) *Nonlinear finite elements for continua and structures*, 2nd edn. John Wiley and Sons, Chichester
51. Simo JC, Hughes TJR (1998) *Computational inelasticity*. Springer, New York

Publisher's Note Springer Nature remains neutral with regard to jurisdictional claims in published maps and institutional affiliations.